




Structural and magnetic phase transitions in Fe₃Ge: A neutron diffraction studyAnatoly M. Balagurov ^{1,2,3} Nataliya Yu. Samoylova ¹ Sergey V. Sumnikov,^{1,2}
Valeria V. Palacheva,^{1,2} and Igor S. Golovin ^{1,2,4}¹Joint Institute for Nuclear Research, 141980 Dubna, Russian Federation²National University of Science and Technology "MISIS," 119049 Moscow, Russian Federation³Lomonosov Moscow State University, 119991 Moscow, Russian Federation⁴Moscow Polytechnic University, 107023 Moscow, Russian Federation

(Received 2 May 2023; accepted 26 May 2023; published 23 June 2023)

A detailed neutron diffraction study of a stoichiometric Fe₃Ge alloy with different initial states in a wide temperature range (up to 1000 K) made it possible to accurately reveal the features of magnetic and structural phase transformations in it. The use of complementary x-ray diffraction and analysis of neutron diffraction patterns by the Rietveld method allowed reliably separating the nuclear and magnetic contributions to the intensity of the diffraction peaks and performing refinement of the Fe₃Ge magnetic state characteristics. Both main phases appearing in Fe₃Ge are ferromagnetic with $T_C = 629$ K (hexagonal, $D0_{19}$) and $T_C = 714$ K (cubic, $L1_2$). In $D0_{19}$, the presence of a spin-flip transition ($T_{sf} = 385$ K) was confirmed and the temperature dependence of the components of magnetic moment along the hexagonal axis and in the basal plane was obtained. It was shown that the transformation between ordered $L1_2$ and $D0_{19}$ structural states, predicted by the equilibrium-phase diagram, includes three steps: two diffusional stages ($L1_2 \rightarrow A1$, $A3 \rightarrow D0_{19}$) and one displacive stage ($A1 \rightarrow A3$). The obtained structural data suggest that in Fe-Ge, as well as in Fe-Ga alloy, direct transitions between ordered phases are impossible. They should include a transition between disordered states.

DOI: [10.1103/PhysRevMaterials.7.063603](https://doi.org/10.1103/PhysRevMaterials.7.063603)

I. INTRODUCTION

Recently, interest in studying the structural properties of various iron-based binary alloys is mainly associated with elucidating their similarities or differences with the properties of Fe-Ga alloys, in which the effect of giant magnetostriction was discovered in the early 2000s. In particular, this applies to Fe-Al, Fe-Ge, and Fe-Si alloys, for which their structural and magnetostrictive properties are compared with those of Fe-Ga in many papers, including one of the first reviews on this topic [1]. A more detailed quantitative comparison of the magnetostrictive properties of binary alloys at the level of tetragonal magnetostriction constants $(3/2)\lambda_{100}$, and energies of magnetoelastic coupling was performed in Ref. [2]. From the data given in this paper, it follows that the maximum value of the positive magnetostriction constant of the Fe-Ge alloy is ~ 2 and ~ 3 times less than that of the Fe-Al and Fe-Ga alloys, respectively, and only slightly larger than that of Fe-Si (all alloys were in slow-cooled state). In the same paper, it was shown that in three types of alloys (Fe-Ga, Fe-Al, and Fe-Ge), the maximum $(3/2)\lambda_{100}$ was reached in the concentration region of the iron-substituting element corresponding to the transition between the disordered and ordered states of the crystal structure. The mentioned features have not yet been properly understood; accordingly, an in-depth study of the details of the structural states of these alloys is required.

For the Fe₃Ge intermetallic compound, another interesting point is the structural transition between the face-centered cubic phase $L1_2$ (structure prototype: Cu₃Au) and the hexagonal phase $D0_{19}$ (structure prototype: Ni₃Sn). According to the known equilibrium phase diagrams [3,4], in a narrow

concentration range (24–26 at. % Ge) at room temperature (RT), this composition should be in the two-phase state $D0_3$ (structure prototype: BiF₃) + $B8_2$ (structure prototype: Ni₂In), which, if heated, first transforms (at 673 K) into $L1_2$, and then (at 973 K) into $D0_{19}$. Both close-packed phases ($L1_2$ and $D0_{19}$) are ordered versions of the disordered A1 (structure prototype: Cu) and A3 (structure prototype: Mg) structures, and, unlike the well-studied transition $A1 \rightarrow A3$, the details and kinetics of the transition between $L1_2$ and $D0_{19}$ structures are not fully known. As will be shown below, in the Fe₃Ge alloy, in some temperature intervals, the coexistence of ordered and disordered states of face-centered cubic structures ($L1_2 + A1$, from now referred to as fcc) and hexagonal close-packed structures ($D0_{19} + A3$, from now referred to as hcp) is possible.

It has been suggested several times in the literature that the formation of the $D0_{19}$ phase from a structure with an fcc lattice should proceed through intermediate disordered states. For example, in Ref. [5] the application of x-ray-diffraction (XRD) and transmission electron microscopy (TEM) methods hinted that the transformation between $L1_2$ and $D0_{19}$ phases in the CoCrTa alloy is a combination of displacive and diffusional atomic rearrangement with an intermediate $A1 \rightarrow A3$ transition between disordered structures. A similar situation occurs for the transition between the ordered $D0_3$ and $L1_2$ phases in the Fe₃Ga alloy. Based on neutron diffraction (ND) data, it was suggested in Ref. [6] and later justified in Ref. [7] that the $D0_3 \rightarrow L1_2$ transformation does not proceed directly, but through the disordered A2 and A1 phases, namely, the sequence $D0_3 \rightarrow A2 \rightarrow A1 \rightarrow L1_2$ being implemented. This means that the

transformation of $D0_3$ into $L1_2$ is a complex one of the diffusional/displacive type combining diffusion ($D0_3 \rightarrow A2$ and $A1 \rightarrow L1_2$) and displacive ($A2 \rightarrow A1$) stages. Accordingly, it is interesting to what extent such a scheme is applicable to the transition between ordered close-packed phases in Fe_3Ge alloy.

The magnetic properties of Fe_3Ge are most fully described in Refs. [8,9], where the susceptibility, magnetization curves, and Mössbauer spectra were measured (see also Ref. [10]). In the hexagonal phase $D0_{19}$, the magnetic state is ferromagnetic (FM) with a Curie temperature $T_C \approx 640$ K and with an iron magnetic moment of about $2.0 \mu_B$ at RT [8]. For this structure, a plane-to-axis spin-reorientation transition ($T_{sr} \approx 380$ K) was also reported [8,9]. The coexisting cubic phase $L1_2$ is also ferromagnetic with $T_C = 740$ K and $\mu_{\text{Fe}} = 2.2 \mu_B$ at RT [8]. At temperature above 750 K, this alloy is obviously in a paramagnetic (PM) state. Neutron diffraction studies of the magnetic structure have been done for Fe_3Ge_2 (ferromagnet, $T_C \approx 470$ K [11]) and FeGe (collinear antiferromagnet, Néel temperature $T_N \approx 410$ K [12]) intermetallics, but they have not yet been performed for Fe_3Ge .

This paper presents results obtained in neutron- and x-ray-diffraction experiments with the Fe_3Ge alloy subjected to various temperature regimes. The analysis of neutron diffraction patterns measured *in situ* during continuous heating up to 1000 K, subsequent exposure and cooling down to RT, and high-resolution diffraction patterns measured at certain fixed temperatures made it possible to exhaustively characterize the features of the emerging structural and magnetic states.

II. SAMPLES, EXPERIMENTS, AND DATA PROCESSING

The Fe-Ge alloy was produced by rapid solidification in a copper mold using Fe (of commercial purity) and Ge (99.99%) by induction melting under the protection of high-purity argon gas in an Indutherm MC-20 V furnace. Using energy-dispersive spectroscopy, the chemical composition of the cast button was confirmed as 25.9 at. % of Ge, which is very close to the stoichiometric 3:1 composition and hereinafter referred to as Fe_3Ge . Rectangular samples $4 \times 8 \times 30$ mm in size were cut from the ingot. The diffraction patterns were measured on three samples: in the initial state after casting (hereinafter referred to “as cast”), after exposure for 24 h at 873 K and quenching in water (hereinafter referred to “annealed-24”), and after exposure for 48 h at 873 K and quenching in water (hereinafter referred to “annealed-48”).

The dependence of magnetization (M) on temperature in the range of 300–1000 K in an external magnetizing field of 5 kOe was measured by a vibrating sample magnetometer VSM-130 with heating and cooling rates of 6 K/min. Curves for the as-cast and annealed-48 samples are shown in Fig. 1. As will be shown below, before heating, in the as-cast sample there are two FM structural phases, $B8_2$ and $D0_{19}$, with T_C values of about 470 and 630 K, accordingly, that also exist after heating-cooling. In the annealed-48 sample there are three FM structural phases ($B8_2$, $D0_{19}$, and $L1_2$) with T_C of about 470, 630, and 730 K, accordingly. Only two of them persist after heating-cooling. Signs of these transitions are clearly seen in Fig. 1.

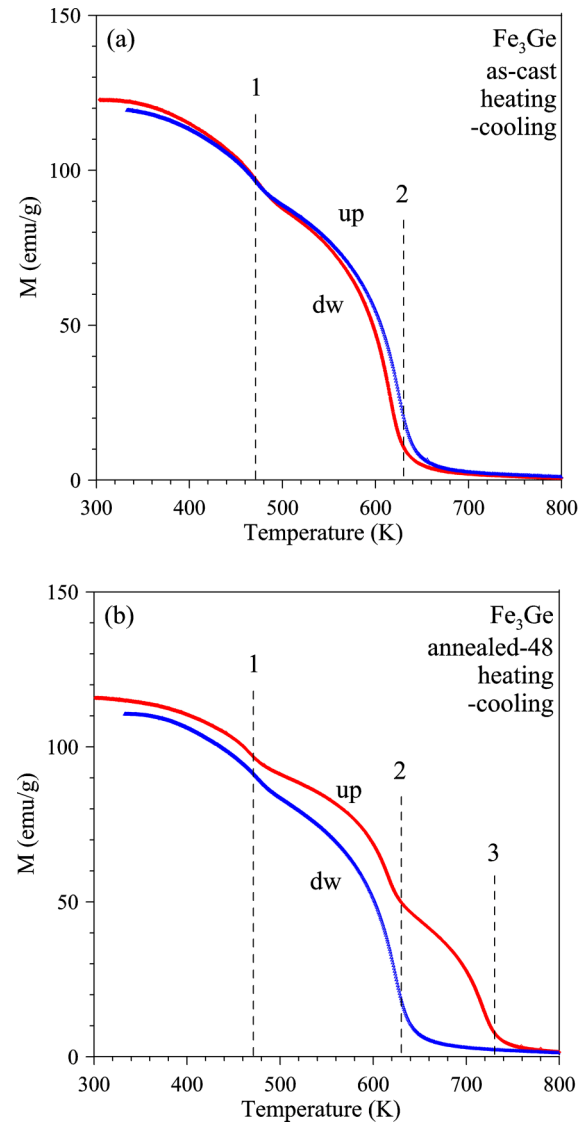


FIG. 1. Temperature dependencies of the specific magnetization during heating (up, red curve) and cooling (dw, blue curve) at a rate of 6 K/min for the as-cast (a) and annealed-48 (b) samples. Dashed lines indicate (conditionally) the FM \leftrightarrow PM transition temperatures for $B8_2$ (1), $D0_{19}$ (2), and $L1_2$ (3).

The neutron diffraction spectra were measured on a time-of-flight (TOF) correlation diffractometer high-resolution Fourier diffractometer (HRFD) [13] operating at the IBR-2 pulsed reactor at Joint Institute for Nuclear Research (JINR) (Dubna). High-resolution TOF spectra were measured for all samples ($\Delta d/d \approx 0.0015$, exposition time 1 h). They were used to determine the phase state, analyze the profiles of diffraction peaks, and accurately determine the unit-cell parameters. The diffraction spectrum measured in the high-resolution mode on the as-cast sample is shown in Fig. 2. The dominant phase in the sample is the structurally ordered phase $D0_{19}$, which is recognized by the presence of superstructure peaks with odd Miller indices h and k (100, 101, 110, etc.). Approximately 10 vol. % of the $B8_2$ structure is also detected in this sample.

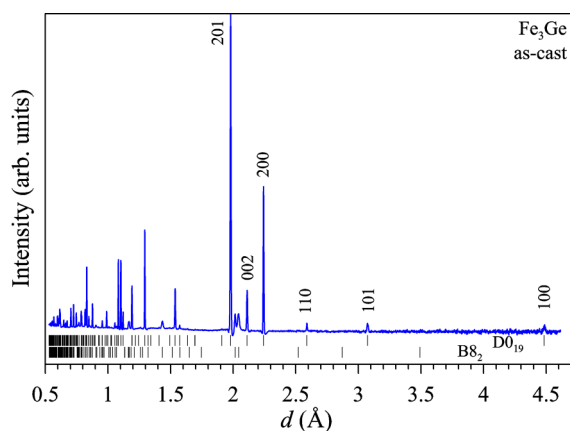


FIG. 2. High-resolution neutron diffraction spectrum of Fe_3Ge in the as-cast state, measured at RT. Vertical ticks indicate calculated peak positions of the main $D0_{19}$ and subsidiary $B8_2$ phases. Miller indices of several high- d peaks of the $D0_{19}$ phase are specified. Small negative dips at both sides of the peak profiles are associated with special features of the high-resolution correlation mode of data acquisition at HRFD.

To obtain diffraction data during heating or cooling of the alloys, the HRFD was switched to a high-intensity medium-resolution mode ($\Delta d/d \approx 0.015$) with an exposure time of 1 min for the entire spectrum. The temperature was increased

(up to ~ 1000 K) and then continuously lowered with a constant rate of 2 K/min. On cooling, the diffraction spectra were measured at certain fixed temperatures to observe possible relaxation processes. Phase transformations that occur with temperature changes or exposures are clearly visible on 2D maps of diffraction spectra. An example of such a map is presented in Fig. 3, which shows the changes of the diffraction spectra of the annealed-48 sample. This sample was heated up to 1000 K, annealed for 1 h, cooled down to 873 K, annealed for 4 h, and finally cooled down to RT. Temperature variations are shown in Fig. 3 and in more detail in Fig. S1 in the Supplemental Material [14].

Since structures $D0_{19}$ and $L1_2$ are ferromagnetic up to several hundreds of kelvin; they make a magnetic contribution to all the intensities of the fundamental and superstructure diffraction peaks. To separate structural and magnetic effects, x-ray-diffraction patterns were measured in both *ex situ* (at RT) and *in situ* (during continuous heating up to 1070 K with a rate of 2 K/min) modes. Co- K_α radiation ($\lambda \approx 1.789$ Å), the penetration depth of which into iron-based alloys is ~ 4 times greater than Cu- K_α radiation, was used on a PANalytical Empyrean diffractometer equipped with a high-efficiency position-sensitive Pixel3D detector. An iron filter was used to suppress K_β radiation. An example of the XRD pattern of the annealed-24 sample is shown in Fig. S2 [14]. All superstructure peaks of both main phases ($D0_{19}$ and $L1_2$) are clearly visible, which means that in addition to magnetic

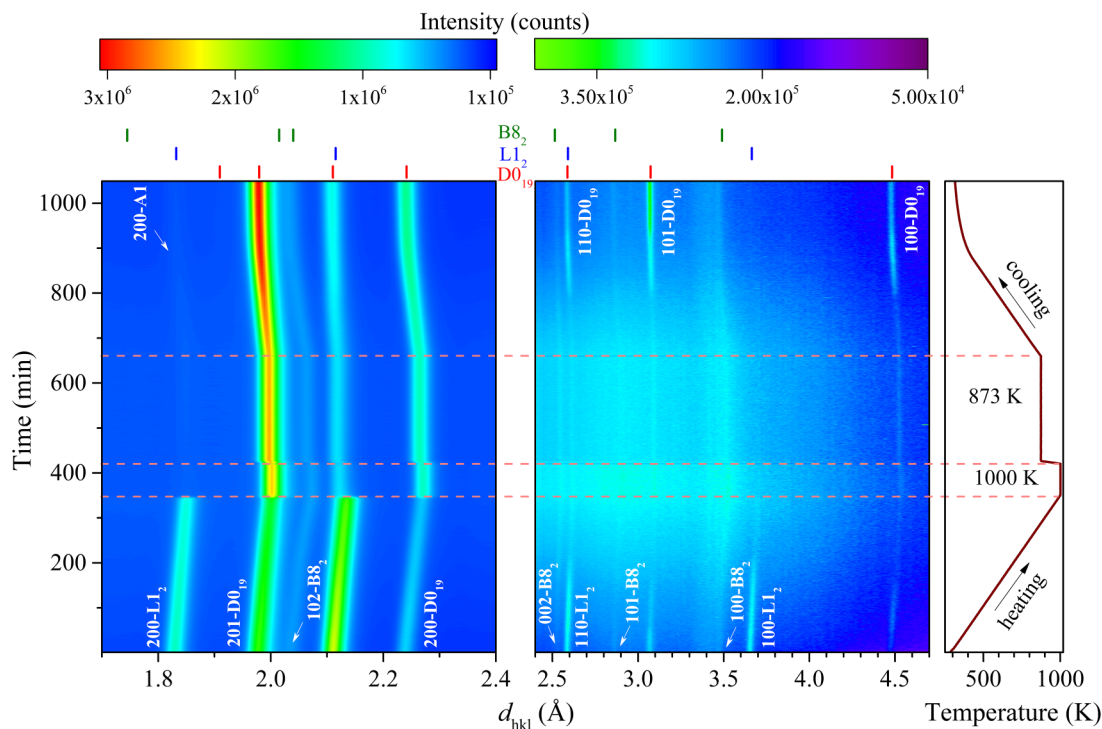


FIG. 3. The 2D map of the evolution of the neutron diffraction patterns of the annealed-48 Fe_3Ge sample measured *in situ* mode upon: continuous heating up to 1000 K (2 K/min), exposure at this temperature for 1 h, cooling down to 873 K, exposure at this temperature for 4 h, and cooling down to RT (2 K/min). Temperature (on the right) and time (on the left) axes go from bottom to top; d -spacing axis goes from left to right. At RT the sample is in the three-phase ($D0_{19} + L1_2 + B8_2$) state, which is characterized by several characteristic fundamental and superstructure diffraction peaks. Final (after cooling down to RT) state is almost pure $D0_{19}$ phase. Measurement time of one spectrum was 1 min; in total, 2D map contains about 1000 patterns. Map is divided into two parts due to strong difference in intensities of fundamental (left part) and superstructure (right part) peaks. Corresponding scale bars are shown above plots.

one there is a well-designed atomic order in these structural states.

Quantitative processing of the measured spectra consisted of determining the temperature dependencies of the integrated intensities, positions, and breadths of several fundamental and superstructure peaks (FITYK [15] software packages was used). These data were then translated into temperatures of structural and magnetic transitions, into volume fractions of structural phases, and parameters of their unit cells. For the analysis of weak superstructure peaks, the diffraction spectra were summed by 4, i.e., for them the effective exposure time was 4 min. The Rietveld method (FULLPROF program [16] with the internal tables for neutron scattering lengths and magnetic form factors) was used for the refinement of the magnetic contribution to the diffraction intensities, which made it possible to determine the temperature dependences of the ordered magnetic moments of the FM phases. Due to strong correlations between some free parameters, it was necessary to increase the measured statistics, so the diffraction spectra were summed by 10 before processing.

To interpret the observed changes in the intensities of the diffraction peaks of different phases, it should be taken into account that, assuming the absence of grain preferred orientations, the integrated intensities of the fundamental (I_F) and superstructure (I_S) peaks depend on temperature as

$$I_F \sim V(T)j_{hkl}L_{hkl}|F_F|^2, I_S \sim V(T)j_{hkl}L_{hkl}\xi^2(T)|F_S|^2, \quad (1)$$

where $V(T)$ is the volume fraction of the phase, L_{hkl} is the Lorentz factor ($L_{hkl} \sim d_{hkl}^4$ for TOF diffraction), j_{hkl} is the multiplicity, (hkl) is a particular set of Miller indices, F_F and F_S are structure factors of fundamental and superstructure peaks, respectively, and $\xi(T)$ is the degree of atomic ordering, $0 \leq \xi(T) \leq 1$. The structure factors include the Debye-Waller factor, $e^{-W_j(T)}$, which can be different for Fe and Ge and where both thermal and static atomic displacements are considered. In the case of unpolarized neutron beam scattering on a ferromagnet, the nuclear, F_N , and magnetic, F_M , structural factors add up quadratically (the interference term vanishes):

$$I_{hkl} \sim F_{hkl,N}^2 + F_{hkl,M}^2. \quad (2)$$

Nuclear and magnetic contributions to the intensities of the diffraction peaks can be easily estimated. For example, in the $L1_2$ phase of Fe_3Ge compound Fe and Ge atoms are in positions $(3c)$ $(0, \frac{1}{2}, \frac{1}{2})$ and $(1a)$ $(0, 0, 0)$, respectively, and the Fe magnetic moment is about $2.2 \mu_B$. Simple calculations of structural factors lead to the following expressions:

$$\begin{aligned} F_{FN} &= 3b_{\text{Fe}} + b_{\text{Ge}}, & F_{SN} &= b_{\text{Fe}} - b_{\text{Ge}}, \\ F_{FM} &= 3b_M, & F_{SM} &= b_M, \end{aligned} \quad (3)$$

where $b_{\text{Fe}} = 0.945$ and $b_{\text{Ge}} = 0.819$ are nuclear coherent scattering lengths for Fe and Ge; $b_M \approx 0.36$ is magnetic scattering amplitude of Fe atoms (all b values are in units of 10^{-12} cm). The calculation of b_M was made assuming that the magnetic form factor is equal to 0.75 for 110 diffraction peak

at $d_{110} = 2.6 \text{ \AA}$, and averaging over equivalent reflections in a cubic lattice was carried out. It follows from (2) and (3) that

$$F_F^2 = (3b_{\text{Fe}} + b_{\text{Ge}})^2 + (3b_M)^2, \quad F_S^2 = (b_{\text{Fe}} - b_{\text{Ge}})^2 + b_M^2, \quad (4)$$

and substituting numbers, the following values can be obtained for individual terms:

$$\begin{aligned} F_{FN}^2 &= 13.35, & F_{FM}^2 &= 1.17, & F_F^2 &= 14.52, \\ F_{SN}^2 &= 0.016, & F_{SM}^2 &= 0.13, & F_S^2 &= 0.146, \\ F_F^2/F_S^2 &\approx 100, & F_{SM}^2/F_{SN}^2 &\approx 8. \end{aligned}$$

A comparison of particular peak intensities should also include the Lorentz factor. Its consideration makes the difference in the intensities of fundamental and superstructure diffraction peaks less dramatic; for example, for 200 and 100 peaks supposing the full order, $\xi(T) = 1$, the intensity ratio is $I_F(200)/I_S(100) = 100/2^4 \approx 6$. For the $D0_{19}$ phase, the situation is about the same, except that in a hexagonal lattice the averaging factor strongly depends on a particular set of Miller indices. From these calculations one can conclude that the observation of superstructure peaks in Fe_3Ge is difficult for both $D0_{19}$ and $L1_2$ phases, and at RT the magnetic contribution to their intensity is noticeably higher than the nuclear one.

The dependence of the Debye-Waller factor on temperature and d_{hkl} is described by the formula $D(T, d) = \exp[-B(T)/(4d^2)]$. Analysis of the high-resolution neutron spectra showed that at room temperature $B(T) \approx 0.4 \text{ \AA}^2$ and in the d_{hkl} range from 1 to 4 \AA , the deviation of $D(T, d)$ from unity does not exceed 10%. The magnetic form factor rapidly decreases with d_{hkl} ; therefore, a significant magnetic contribution to the intensity of diffraction peaks is present only if $d_{hkl} > 2 \text{ \AA}$.

III. RESULTS

A. Initial and final (after heating-cooling cycle) structural states

According to Refs. [3,4], below 673 K, the Fe_3Ge alloy transforms into the cubic phase $D0_3$ ($Fm\bar{3}m$) and the hexagonal phase $B8_2$ ($P6_3/mmc$). However, in our samples, as follows from the ND high-resolution data (Fig. 2), in the as-cast state, the main phase is metastable at RT $D0_{19}$ ($P6_3/mmc$). The structure of the stoichiometric composition of this phase can be completely ordered; all atoms are in $(2a)$ and $(6h)$ special positions, Ge and Fe, respectively. Ordering leads to a doubling of the unit-cell parameters of the initial disordered phase $A3$ in the plane and the values are $a \approx 5.185 \text{ \AA}$ and $c \approx 4.225 \text{ \AA}$, with $N = 8$ atoms per unit cell. The $B8_2$ phase ($a \approx 4.030 \text{ \AA}$, $c \approx 5.028 \text{ \AA}$, and $N = 6$) content is relatively low (~ 10 vol. %). The atomic structure of this defective phase for the composition $\text{Fe}_{3.34}\text{Ge}_2$ is described in Ref. [11] in detail. In this work the magnetic characteristics of the $B8_2$ phase are provided: Curie temperature, $T_C = 470$ K, which coincides with our data on magnetization (Fig. 1), and iron-ordered magnetic moment, $\mu_{\text{Fe}} \approx 1.7 \mu_B$.

After the first annealing (24 h at 873 K) and subsequent water quenching, the $L1_2$ phase was formed ($\sim 10\%$ of the sample volume, cubic structure, $Pm\bar{3}m$, $a \approx 3.664 \text{ \AA}$, and $N = 4$). Additional annealing (48 h at 873 K) followed by water

TABLE I. Observed structural and magnetic states in annealed-48 sample during heating to 1070 K and subsequent cooling to RT after additional isothermal annealing of sample at 873 K during 4 h. At heating, volume fractions of both DO_{19} and $L1_2$ phases are close to 50% up to 978 K. At cooling, $L1_2$ phase is practically absent.

State	Heating		Cooling	
	T range, K	hcp	fcc	hcp
I	<385	DO_{19} , FM, (μ_x, μ_z)	$L1_2$, FM, μ_x	
II	385–629	DO_{19} , FM, μ_z	$L1_2$, FM, μ_x	<340
III	629–714	DO_{19} , PM	$L1_2$, FM, μ_x	382–340
IV	714–978	DO_{19} , PM, ~50%	A1, PM, ~50%	621–382
V	978–1070	DO_{19} + A3, PM	A1, PM, <2%	1070–621

quenching leads to an increase in the fraction of the $L1_2$ phase to almost ~50%.

The evolution of x-ray-diffraction patterns during the heating process of the annealed-24 sample is shown in Fig. S3 in the Supplemental Material [14]. The superstructure peaks of the DO_{19} phase (101 and 110) remain clearly visible up to 1070 K. In addition, despite helium atmosphere, the oxidation process took place and quite intensive diffraction peaks of Fe_3O_4 oxide appeared at high temperature. Intensive x-ray-diffraction peaks of the $L1_2$ phase are outside the measured range of scattering angles in Fig. S3 [14], but in the neutron 2D map (Fig. 2) it is clearly visible that this phase fully disappears at around 1000 K. The peaks of the $B8_2$ phase are present up to highest temperatures in both neutron- and x-ray-diffraction patterns.

High-resolution diffraction spectra were measured for the annealed-48 sample before it was heated to 1000 K and after subsequent cooling (see Fig. S4 in the Supplemental Material [14]). In the ND pattern measured before heating, the peaks of both structures (DO_{19} and $L1_2$) are recorded. After cooling, the main structure is DO_{19} , all superstructure peaks of the $L1_2$ structure disappeared, and only a couple of weak peaks from the A1 phase are recorded (especially, peak 200 is visible). As for the $B8_2$ phase, after cooling its fraction in the sample volume is practically the same as in the state before heating.

B. Phase transitions during heating and cooling

Based on the results obtained by x-ray- and neutron diffraction during heating-exposure-cooling procedure of the annealed-48 sample, five different states have been distinguished in the temperature range from 300 to 1070 K (Table I).

The hcp phase is ferromagnetic up to ~629 K; the change in the easy-magnetization direction from the plane to the axis occurs at approximately 385 K. According to the equilibrium-phase diagram [3], this phase retains a high degree of the Fe and Ge ordering up to ~1400 K. The fcc phase is ordered ferromagnetic up to ~714 K; at higher temperatures it is paramagnetic and disordered (the $L1_2 \rightarrow A1$ transition takes place). The fcc ($A1$) \rightarrow hcp ($A3$) transition is observed at ~978 K. These states and transitions are illustrated in Figs. 4–6.

In Fig. 4 the temperature dependencies of the fundamental diffraction peak intensities are shown during heating and subsequent cooling. From these dependencies the volume fractions of the fcc and hcp phase can be easily obtained. During the heating of the annealed-48 sample, both main phases

(hcp and fcc) are present in approximately equal amounts. A gradual decrease in the intensities of their characteristic diffraction peaks is associated with the temperature dependence of the Debye-Waller factor. As can be seen in Fig. 4, none of the transformations mentioned in Table I manifest themselves in any way; only the fcc \rightarrow hcp transition at $T \approx 978$ K is clearly visible. On the contrary, in the temperature dependencies of the intensities of the superstructure peaks, the transformation between structural and magnetic states appears very clearly (Fig. 5).

First, it can be seen that the change of the magnetization direction in the DO_{19} phase near 380 K leads to noticeable changes in the intensities of 100 (increasing on heating and decreasing on cooling) and 101 (changes are opposite) peaks. Obviously, this is due to the factor $|\sin \eta_{hkl}|^2$, to which the magnetic contribution to the intensities of the diffraction

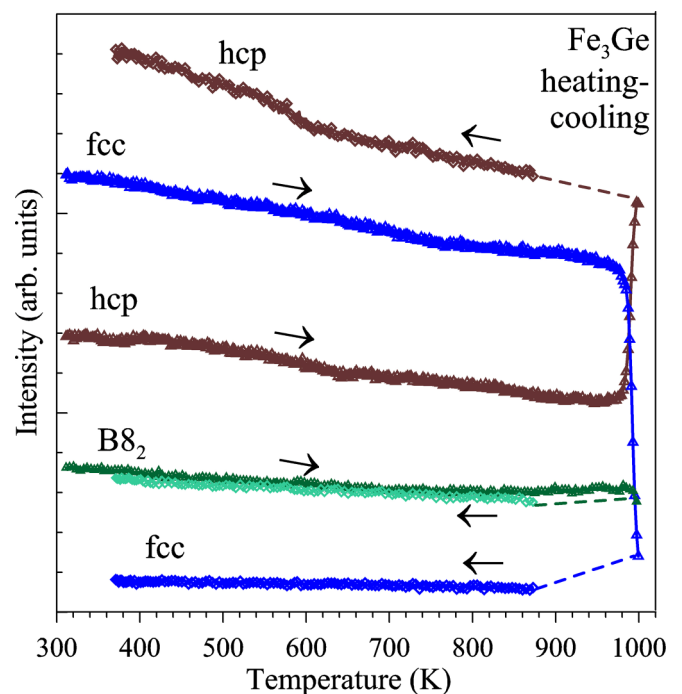


FIG. 4. Intensities of characteristic fundamental neutron diffraction peaks of structural phases present in the annealed-48 sample of Fe_3Ge upon its heating up to 1000 K (arrows point left to right) and cooling down to RT (arrows point right to left) after annealing at 873 K in 4 h.

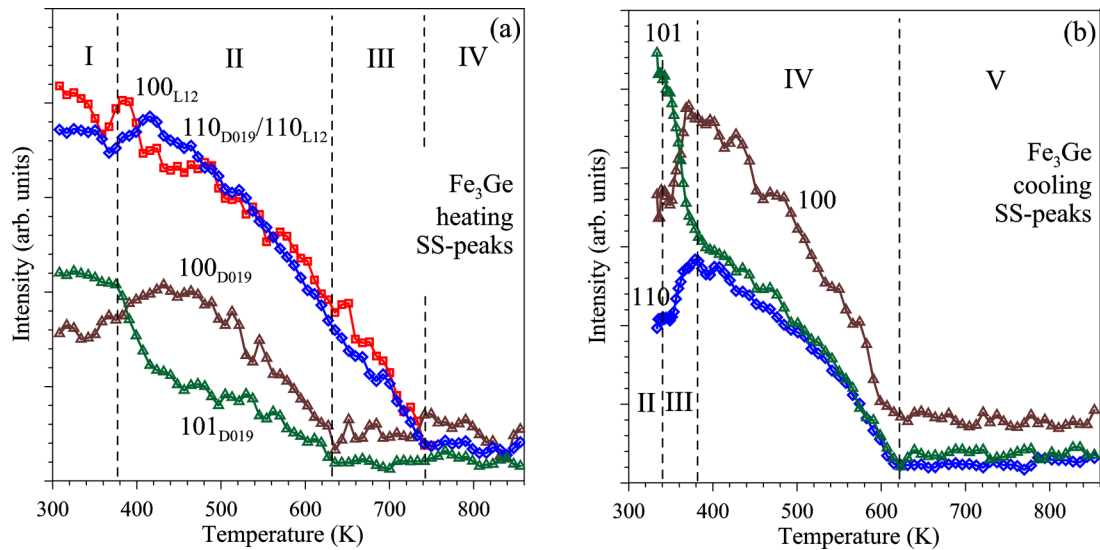


FIG. 5. Intensities of characteristic superstructure neutron diffraction peaks in annealed-48 Fe_3Ge sample measured upon heating (a) and subsequent cooling (b). At heating, both $D0_{19}$ and $L1_2$ phases are present in shown temperature range. At cooling, the $L1_2$ phase is absent, and all Miller indices are attributed to $D0_{19}$. Types of structural and magnetic states are indicated according to Table I.

peaks is proportional, $I_{hkl,M} \sim |\sin \eta_{hkl}|^2$ (see, for instance, Ref. [17]). Here, η_{hkl} is the angle between the direction of the magnetic moment of the atom and the scattering vector. The FM \leftrightarrow PM transitions in $D0_{19}$ ($T_C = 629$ K on heating, $T_C = 621$ K on cooling) are seen from the disappearance of the magnetic contribution to the intensities of 100 and 101 peaks. All superstructure peaks of the $L1_2$ phase disappear at ~ 743 K, which indicate the transition into disordered A1 state. The FM \rightarrow PM transition in the $L1_2$ phase occurs close to this temperature ($T_C = 714$ K), which is in agreement with the $M(T)$ curves (Fig. 1).

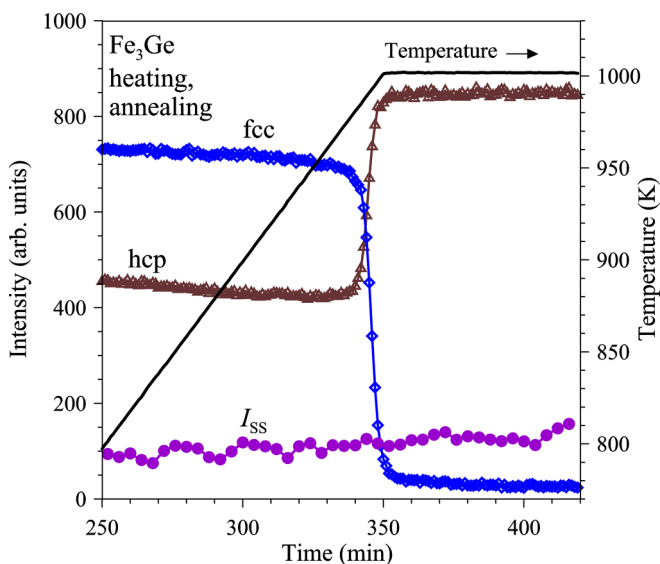


FIG. 6. Time evolution of intensities of 200 fundamental neutron diffraction peaks of fcc and hcp phases and total intensity of several superstructure peaks of $D0_{19}$ phase (I_{SS}) (left axis) of annealed-48 Fe_3Ge sample upon heating up to 1000 K and annealing at this temperature. Temperature variations are also shown (right axis).

The two-phase state ($A1 + D0_{19}$) exists up to $T \approx 978$ K; at this temperature the fcc \rightarrow hcp transition begins, the course of which over time is shown in Fig. 6. A detailed quantitative examination shows that the increase of the $D0_{19}$ content begins at $T = (978 \pm 2)$ K: the increase of its volume fraction to 0.95 occurs in 8 min; reaching a stationary value of 0.98 takes another 10 min. An obvious observed feature of this process is the absence of a distinct increase in the intensity of the superstructure peaks of the hcp phase, despite an increase in its volume fraction in the sample by 2 times. This means that the fcc \rightarrow hcp transition takes place without ordering, forming the A3 structure. Lowering the temperature to 873 K and annealing for 4 h practically does not change the volume fraction of $D0_{19}$; at the end of exposure it decreases by only ~ 0.01 . The content of the A1 phase reaches ~ 0.03 at the end of exposure at 873 K (Fig. S5 [14]), which indicates very high thermal stability to overcooling and sluggish diffusion-controlled $D0_{19}$ to $L1_2$ phase transition. This is a completely different kinetic of this transition compared with the same transition in Fe_3Ga alloys (see Ref. [18] and references therein).

Upon further cooling to RT, the volume fractions of the A1 and $B8_2$ phases did not change much (Fig. 4). At $T_C \approx 621$ K (Fig. 5), the process of magnetic ordering of the $D0_{19}$ phase takes place, which follows from a rapid increase in the intensity of its superstructure peaks. The expected appearance of the $D0_3$ phase, as it is described in Ref. [4], and proposed by equilibrium-phase diagram, was not observed in our *in situ* experiments, confirming sluggish diffusion-controlled eutectoid reaction in this system.

C. Magnetic structures

As mentioned, both phases $D0_{19}$ and $L1_2$ are ferromagnetic, and the Rietveld method was used to separate the structural and magnetic contributions to the intensity of the diffraction peaks and to determine the temperature dependencies

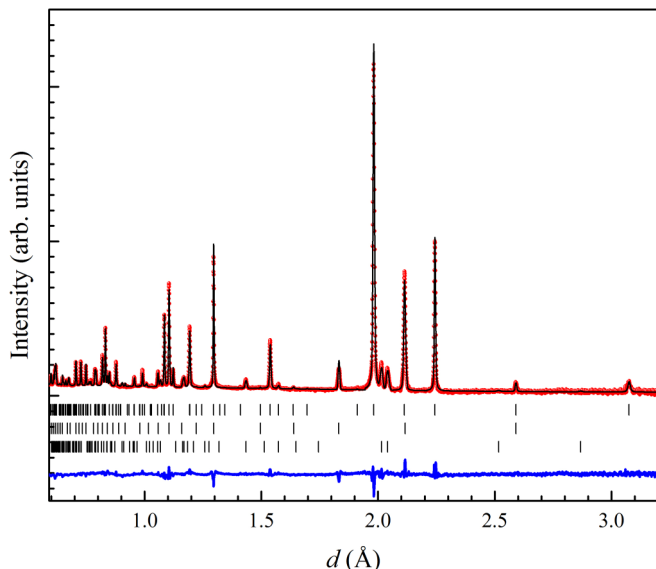


FIG. 7. Neutron diffraction pattern (high resolution) of annealed-24 Fe_3Ge sample collected at RT and processed by the Rietveld method. Experimental points, calculated (red) and difference (blue) lines are shown. Vertical bars are calculated peak positions of DO_{19} , $L1_2$, and $B8_2$ phases (from top to bottom).

of the magnetic moments. The parameters of three structural (DO_{19} , $L1_2$, $B8_2$) and two magnetic (DO_{19} , $L1_2$) phases were refined. The magnetic characteristics of the $B8_2$ phase were not refined due to its overall negligibly small amount in the samples (~ 10 vol. %) and the relatively small value of the ordered magnetic moment ($\mu_{\text{Fe}} \approx 1.7 \mu_{\text{B}}$, [11]), which led to a very small magnetic contribution to the intensity of diffraction peaks. The high- and medium-resolution diffraction spectra

measured *ex situ* were processed together, which improved the statistics and increased the processing reliability. For spectra measured *in situ* with continuous temperature scanning at heating and cooling, only data measured at medium resolution were processed. The refined structural parameters were volume fractions of phases, their unit-cells parameters, isotropic Debye-Waller factors for both Fe and Ge atoms, and the components of the Fe magnetic moment. An example of Rietveld refinement of the high-resolution pattern for annealed-24 sample is shown in Fig. 7. It is evident that the refinement quality is good enough. For high-resolution patterns the χ^2 and R_W values, describing the correspondence between experimental and calculated data, are $\chi^2 \sim 2$ and $R_W \sim 3\%$; for medium-resolution patterns variations of these values are 2.2–4.3 and 3.8–5.2%, respectively. The processing quality did not depend on the specific direction of the DO_{19} magnetic moment in the basal plane, and the direction [100] was used for certainty.

The values of the magnetic moment of Fe atoms obtained during heating and cooling of the annealed-48 sample are shown in Fig. 8, and the numerical data are summarized in Table II. The refined structural characteristics are provided in the Supplemental Material (Table S1) [14]. The temperature dependencies of the magnetic moments were approximated by a phenomenological power-law function for the spontaneous magnetization $\mu(T) = \mu_0[1 - (T/T_C)^\alpha]^\beta$, which is usually true over the entire temperature scale. In this equation, μ_0 is the saturated magnetic moment at $T=0$, T_C is the Curie temperature, and α and β are the refinable exponential parameters. At temperatures close to T_C , this formula is modified to the standard expression $\mu(T) \sim [1 - T/T_C]^\beta$, where the critical exponent β is ~ 0.5 for the mean-field model. For the DO_{19} phase the refined values (T_C , T_{sf} , and μ_{293}) for the heating procedure are in satisfactory agreement with the Mössbauer data reported in Ref. [8] ($T_C = 640$ K, $T_{\text{sf}} = 380$ K, and

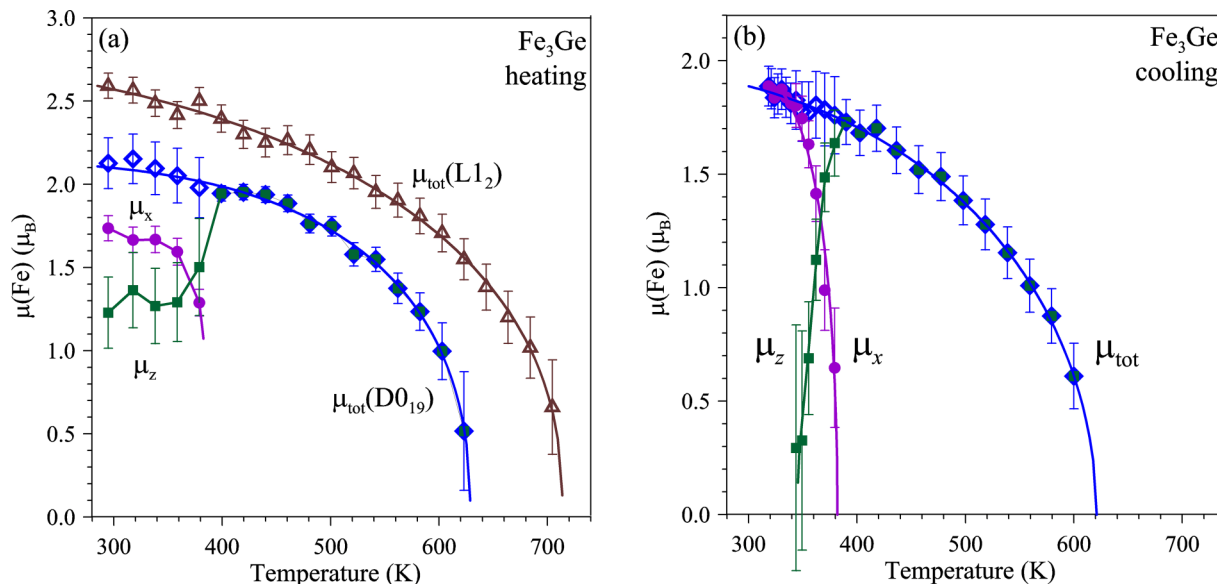


FIG. 8. Temperature dependences of Fe-ordered magnetic moments of DO_{19} and $L1_2$ phases at heating (a) and DO_{19} phase at cooling (b) in annealed-48 sample. For DO_{19} phase, total magnetic moment and its components in basal plane (μ_x) and along hexagonal axis (μ_z) are shown. Lines through total magnetic moment are drawn according to phenomenological power-law function (see text). Lines through μ_x and μ_z points are guides for the eyes.

TABLE II. Summary of magnetic characteristics of Fe₃Ge alloy (annealed-48 sample) obtained during heating and cooling and approximated by the relation $\mu(T) = \mu_0[1 - (T/T_C)^\alpha]^\beta$. T_C and T_{sf} are Curie and spin-flip transition temperatures, μ_0 and μ_{293} are total ordered magnetic moments at $T = 0$ and 293 K. Numbers in parentheses are statistical errors with respect to the last significant digit.

Quantity	Heating		Cooling
	$L1_2$	$D0_{19}$	$D0_{19}$
T_C , K	714(7)	629(9)	621(8)
T_{sf} , K		385(10)	382(4)
μ_0, μ_B	2.80(10)	2.20(10)	2.02(5)
μ_{293}, μ_B	2.59(7)	2.12(7)	1.89(9)
α	2.1(5)	4(1)	2.9(6)
β	0.41(6)	0.41(10)	0.51(8)

$\mu_{293} = 2.03$), whereas for the $L1_2$ phase the differences are far beyond the possible errors ($T_C = 740$ K and $\mu_{293} = 2.21$).

For the parameters of the elementary cells of the $D0_{19}$ and $L1_2$ phases refined by the Rietveld method, the average coefficients of linear thermal expansion in the temperature range (300–800) K are 17×10^{-6} for a parameter of $L1_2$, 19×10^{-6} and 7×10^{-6} (in K^{-1} units) for a and c parameters, accordingly, of $D0_{19}$. The effect of spontaneous magnetostriction can be traced only for the hexagonal axis of the $D0_{19}$ phase. The relative “jump” of the c parameter is small ($\Delta c/c \approx 0.0005$) but it is clearly seen, especially for the c/a ratio. The correlation of this effect with the formation of the FM structure is shown in Fig. 9.

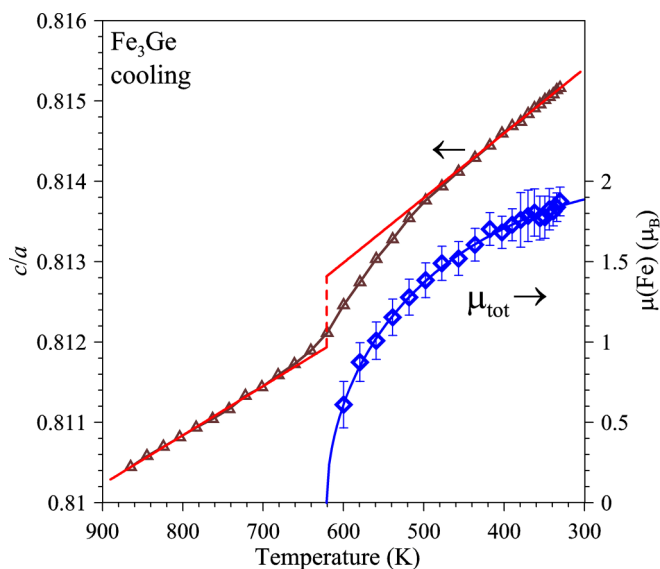


FIG. 9. Temperature dependencies of total magnetic moment obtained at cooling (right axis) of Fe₃Ge in annealed-48 state and ratio c/a of unit-cell parameters (left axis). Straight lines are a description of cell parameters by linear functions. The “jump” of the ratio shown by a vertical line coincides with appearance of FM order in $D0_{19}$ phase.

The Curie and spin-flip transition temperatures indicated in Table II generally correspond well to our magnetization data (Fig. 1) and the data published in Refs. [8,9].

IV. DISCUSSION

According to the results presented in this paper, neither in the as-cast state nor after a relatively long annealing at 873 K does the phase composition of the Fe₃Ge intermetallic compound correspond to the equilibrium phase diagram. According to Refs. [3,4], at RT this compound should be in the two-phase $D0_3 + B8_2$ state, which, when heated, first transforms (at 673 K) into $L1_2$, and then (at ~ 973 K) into $D0_{19}$. As clearly follows from the neutron diffraction data, in the as-cast state (rapid cooling of a 50-g ingot in a copper mold), only the high-temperature phase $D0_{19}$ is detected in the sample. Annealing at 873 K for 24 and 48 h leads to the transition of part of this structure ($\sim 10\%$ after 24 h and $\sim 50\%$ after 48 h) to $L1_2$, i.e., the $D0_{19} \rightarrow L1_2$ transformation rate upon annealing is rather slow. This feature of Fe₃Ge was noted in Ref. [19], where $D0_{19} \leftrightarrow L1_2$ transitions were studied at the level of microstructure changes (electron backscatter diffraction (EBSD) and TEM methods). Also, it was noticed that the transition between disordered states of these phases ($A3 \rightarrow A1$) and the transition $L1_2 \rightarrow D0_{19}$ at heating are much faster compared to the $D0_{19} \rightarrow L1_2$ transition at cooling.

The annealed-48 sample is characterized by a two-phase structure ($L1_2 + D0_{19}$) with practically equal phase-volume fractions. During heating, $\sim 50\%$ of the volume occupied by the $L1_2$ phase transforms into the disordered $A1$ phase, then (at 978 K) in this part of the sample volume $fcc \rightarrow hcp$ transformation occurs quite quickly. This transformation proceeds without ordering (the $A3$ phase appears); only some subtle tendency of increasing of superstructure peak intensities is visible in Fig. 6. Perhaps, with a longer exposure at 1000 K, ordering of the $A3$ phase, i.e., the $A3 \rightarrow D0_{19}$ transformation, would be more noticeable. Such a sequence of transitions confirms the assumptions (e.g., Refs. [5,20]) about the need for an intermediate disordered hcp state during the formation of the $D0_{19}$ phase from a structure with fcc lattice. This means that the transformation from $L1_2$ into $D0_{19}$ is not direct, but has a complex nature combining diffusion (starting $L1_2 \rightarrow A1$ and final $A3 \rightarrow D0_{19}$) and intermediate displacive ($A1 \rightarrow A3$) stages.

The transformation between the states $L1_2$ and $D0_{19}$ during continuous heating was also observed in Fe- x Ga alloys with a Ga content of about 25–28 at. %. It can be deduced from the data presented in Ref. [21] that in Fe- x Ga this transformation proceeds much faster than in Fe₃Ge: the transition temperature is lower (~ 903 K instead of ~ 978 K) and the transition temperature range is approximately 2 times shorter. The reason for the slower kinetics of transformations between the fcc ($L1_2$ or $A1$) and hcp ($D0_{19}$ or $A3$) structural states in Fe-Ge (compared to Fe-Ga) could be a higher difference in the atomic volumes, V_a (the fraction of the unit-cell volume per atom): $\sim 0.04 \text{ \AA}^3$ in Fe-Ge and $\sim 0.02 \text{ \AA}^3$ in Fe-Ga (Fig. S6 [14]). This leads to a higher potential barrier for the transition in Fe-Ge and a corresponding slowdown in the kinetics, which was noted in Refs. [4,19]. The volumetric

coefficients of thermal expansion of the fcc and hcp phases (indicated in Fig. S6 [14]) are the same in the two-phase state in the Fe-Ge alloy, slightly different in the Fe-Ga alloy, and approximately correspond to the pure iron.

Another interesting result is the behavior of the ordered magnetic moment of the DO_{19} phase. The presence of spin-reorientation transition from plane to axis ($T_{sr} \approx 380$ K) in the hexagonal Fe_3Ge was known since the middle 1970s from the Mössbauer effect and magnetization measurements [8]. Later, the magnetocrystalline anisotropy of this phase was studied in detail in Ref. [9] and described in terms of the Carr model for localized moments [22]. In the neutron diffraction data, the spin-flip transition is seen clearly from the temperature behavior of the superstructure peak intensities, for which the magnetic contribution is much higher than the nuclear one (Fig. 5). The Rietveld refinement helped to allocate contributions to the total moment from μ_x and μ_z components and showed the absence of the preferred direction in the basal plane. This is consistent with the Mössbauer data showing a random distribution of the moment orientations in the basal plane. There is an error-exceeding difference in Curie temperatures determined from neutron and Mössbauer [8] data for both $L1_2$ (714 vs 740 K) and DO_{19} (629 vs 640 K) phases, which can be attributed to some difference in the germanium content in the alloys.

V. CONCLUSIONS

Neutron diffraction experiments were performed on the Fe-Ge alloy with the composition close to stoichiometric Fe_3Ge and underwent different temperature treatments. The real-time analysis of structural and magnetic phase transitions during heating (up to 1000 K) and subsequent cooling was carried out. At RT, the $B8_2$ state, predicted by the equilibrium-phase diagram, was observed only in a small amount (~ 10 vol. %), and its volume fraction in the samples is practically independent of their initial state (as cast or annealed) and remains constant upon heating up to 1000 K and subsequent cooling. In the as-cast sample, the DO_{19} is the dominating phase; in the structure of the studied sample over the entire temperature range no traces of $L1_2$ were found.

In the sample annealed for 48 h at 873 K, the initial state is a three-phase one ($L1_2 + DO_{19} + B8_2$) with the volume fraction ratios 0.46:0.48:0.06. Based on the diffraction data, it can be unambiguously concluded that if the studied sample is heated to 1000 K, only the FM \rightarrow PM ($T_C \approx 629$ K) transition occurs in the DO_{19} phase; no structural transitions are observed. In the $L1_2$ phase, the FM \rightarrow PM transition ($T_C \approx 714$ K) and two structural transitions occur: $L1_2 \rightarrow A1$ ($T_s \approx 743$ K) and $A1 \rightarrow A3$ ($T_s \approx 978$ K). These results suggest that the first-order transition between ordered phases is impossible. First, a disordered phase ($A1$) must appear, then transform into another disordered state ($A3$), from which an ordered state (DO_{19}) can then be formed. A similar sequence of transformation between ordered structures in a Fe-Ga alloy was found for the transformation of DO_3 into $L1_2$: $DO_3 \rightarrow A2 \rightarrow A1 \rightarrow L1_2$ [7], which is also a complex transition combining the diffusional and displacive stages.

The obtained neutron diffraction data made it possible to identify the magnetic contributions to the intensity of the superstructure peaks of both main phases (DO_{19} and $L1_2$), determine the temperature dependence of the ordered magnetic moment, and confirm the presence of a moment-reorientation transition in the DO_{19} phase from planar to axial when heating and back when cooling. The refined value of the critical exponent β is close to the prediction of the mean-field model.

The results obtained in the real-time mode with continuous heating allowed us to find a possible explanation for the different kinetics of transformations between the fcc and hcp states in Fe_3Ge and Fe_3Ga . It is based on the difference in the atomic volumes of the $A1$ and $A3$ phases, which leads to a higher potential barrier for the $A1 \rightarrow A3$ transition in Fe-Ge and a corresponding slowdown in the kinetics.

ACKNOWLEDGMENTS

The ND experiments were carried out using the IBR-2 (FLNP JINR) neutron source. The authors are grateful to Dr. R. N. Vasin for valuable advices and N. A. Sayapina for her critical reading of the manuscript and helpful suggestions. This work was funded by Russian Science Foundation Project No. 22-42-04404.

-
- [1] E. M. Summers, T. A. Lograsso, and M. Wun-Fogle, Magnetostriction of binary and ternary Fe-Ga alloys, *J. Mater. Sci.* **42**, 9582 (2007).
 - [2] J. B. Restorff, M. Wun-Fogle, K. B. Hathaway, A. E. Clark, T. A. Lograsso, and G. Petculescu, Tetragonal magnetostriction and magnetoelastic coupling in Fe-Al, Fe-Ga, Fe-Ge, Fe-Si, Fe-Ga-Al, and Fe-Ga-Ge alloys, *J. Appl. Phys.* **111**, 023905 (2012).
 - [3] H. Okamoto, Fe-Ge (Iron-Germanium), *J. Phase Equilib. Diffus.* **29**, 292 (2008).
 - [4] K. Biswas, P. K. Das, and K. Chattopadhyay, Microstructural evolution in laser-ablation-deposited Fe-25 at.% Ge thin film, *J. Mater. Res.* **21**, 174 (2006).
 - [5] B. Cheong, Y. C. Feng, and D. E. Laughlin, $L1_2$ to DO_{19} structural ordering during the fcc to hcp transformation in a CoCrTa alloy, *Scr. Metall. Mater.* **30**, 1419 (1994).
 - [6] V. V. Palacheva, A. Emdadi, F. Emeis, I. A. Bobrikov, A. M. Balagurov, S. V. Divinski, G. Wilde, and I. S. Golovin, Phase transitions as a tool for tailoring magnetostriction in intrinsic Fe-Ga composites, *Acta Mater.* **130**, 229 (2017).
 - [7] A. M. Balagurov, N. Yu. Samoylova, I. A. Bobrikov, S. V. Sumnikov, and I. S. Golovin, The first- and second-order isothermal phase transitions in Fe_3Ga -type compounds, *Acta Cryst.* **B75**, 1024 (2019).
 - [8] J. W. Drijver, S. G. Sinnema, and F. Van der Woude, Magnetic properties of hexagonal and cubic Fe_3Ge , *J. Phys. F: Met. Phys.* **6**, 2165 (1976).
 - [9] F. Albertini, D. Negri, L. Pareti, E. B. Watts, Z. Arnold, J. Kamarad, G. Calestani, A. Deriu, and S. Besseghini, Magnetocrystalline anisotropy of Fe_3Ge single crystal: Effect of pressure and Mn substitution for Fe, *J. Appl. Phys.* **96**, 2110 (2004).

- [10] I. S. Golovin, A. M. Balagurov, I. A. Bobrikov, and J. Cifre, Structure induced anelasticity in Fe_3Me (Me = Al, Ga, Ge) alloys, *J. Alloys Compd.* **688**, 310 (2016).
- [11] F. Albertini, L. Pareti, A. Deriu, D. Negri, G. Calestani, O. Moze, S. J. Kennedy, and R. Sonntag, A magnetic and structural study of Mn, Co, and Ni substituted Fe_3Ge_2 hexagonal germanides, *J. Appl. Phys.* **84**, 401 (1998).
- [12] J. Bernhard, B. Lebech, and O. Beckman, Magnetic phase diagram of hexagonal FeGe determined by neutron diffraction, *J. Phys. F: Met. Phys.* **18**, 539 (1988).
- [13] A. M. Balagurov, Scientific reviews: High-resolution Fourier diffraction at the IBR-2 Reactor, *Neutron News* **16**, 8 (2005).
- [14] See Supplemental Material at <http://link.aps.org/supplemental/10.1103/PhysRevMaterials.7.063603> for temperature variations during XRD experiment; XRD pattern of the annealed-24 Fe_3Ge sample; *in situ* XRD patterns of the annealed-24 Fe_3Ge sample; high-resolution neutron diffraction patterns of the annealed-24 Fe_3Ge sample; time evolution of the fcc and hcp phase-volume fractions of the annealed-48 Fe_3Ge sample upon heating; and changes in the atomic volumes of structural phases in the fcc \rightarrow hcp phase-transition region in Fe_3Ga and Fe_3Ge .
- [15] M. Wojdyr, Fityk: A general-purpose peak fitting program, *J. Appl. Cryst.* **43**, 1126 (2010).
- [16] J. Rodriguez-Carvajal, Recent advances in magnetic structure determination by neutron powder diffraction, *Physica B* **192**, 55 (1993).
- [17] G. Shirane, A note on the magnetic intensities of powder neutron diffraction, *Acta Cryst.* **12**, 282 (1959).
- [18] I. S. Golovin, A. M. Balagurov, I. A. Bobrikov, S. V. Sumnikov, and A. K. Mohamed, Cooling rate as a tool of tailoring structure of Fe-(9-33%)Ga alloys, *Intermetallics* **114**, 106610 (2019).
- [19] Q. Z. Chen, A. H. W. Ngan, and B. J. Duggan, The $L1_2 \leftrightarrow D0_{19}$ transformation in the intermetallic compound Fe_3Ge , *J. Mater. Sci.* **33**, 5405 (1998).
- [20] P. A. Carvalho, P. M. Bronsveld, B. J. Kooi, and J. Th. M. De Hosson, On the fcc $\rightarrow D0_{19}$ transformation in Co-W alloys, *Acta Mater.* **50**, 4511 (2002).
- [21] A. M. Balagurov, I. S. Golovin, I. A. Bobrikov, V. V. Palacheva, S. V. Sumnikov, and V. B. Zlokazov, Comparative study of structural phase transitions in bulk and powdered Fe-27Ga alloy by real-time neutron thermodiffraction, *J. Appl. Cryst.* **50**, 198 (2017).
- [22] W. J. Carr Jr., Temperature dependence of ferromagnetic anisotropy, *Phys. Rev.* **109**, 1971 (1958).